Density Functional Study of the ^{13}C NMR Chemical Shifts in Small-to-Medium-Diameter Infinite Single-Walled Carbon Nanotubes

Eva Zurek

Max-Planck-Institut für Festkörperforschung, Heisenbergstrasse 1, 70569 Stuttgart, Germany

Chris J. Pickard

Theory of Condensed Matter (TCM) Group, Cavendish Laboratory, Madingley Road, Cambridge CB3 OHE, United Kingdom

Brian Walczak and Jochen Autschbach*

Department of Chemistry, State University of New York at Buffalo, Buffalo, New York 14260-3000

Received: July 18, 2006

NMR chemical shifts were calculated for semiconducting (n,0) single-walled carbon nanotubes (SWNTs) with n ranging from 7 to 17. Infinite isolated SWNTs were calculated using a gauge-including projector-augmented plane-wave (GIPAW) approach with periodic boundary conditions and density functional theory (DFT). In order to minimize intertube interactions in the GIPAW computations, an intertube distance of 8 Å was chosen. For the infinite tubes, we found a chemical shift range of over 20 ppm for the systems considered here. The SWNT family with $\lambda = \mathrm{mod}(n, 3) = 0$ has much smaller chemical shifts compared to the other two families with $\lambda = 1$ and $\lambda = 2$. For all three families, the chemical shifts decrease roughly inversely proportional to the tube's diameter. The results were compared to calculations of finite capped SWNT fragments using a gauge-including atomic orbital (GIAO) basis. Direct comparison of the two types of calculations could be made if benzene was used as the internal (computational) reference. The NMR chemical shifts of finite SWNTs were found to converge very slowly, if at all, to the infinite limit, indicating that capping has a strong effect (at least for the (9,0) tubes) on the calculated properties. Our results suggest that ^{13}C NMR has the potential for becoming a useful tool in characterizing SWNT samples.

I. Introduction

The properties, separation, and potential applications of carbon nanotubes[1] are currently under intense study. The wide range of proposed applications[2] (e.g., for building molecular transistors[3] and electron field emitters,[4] as artificial muscles,[5] as magnetic tips for magnetic scanning probe microscopy,[6] or for DNA sequencing[7]) stems from the fact that carbon nanotubes have a diverse range of weights, electronic structures, helicities, and so forth. Individual classes of tubes might exhibit significantly different physical and chemical properties. Considerable effort has been placed into determining the experimental parameters that affect the molecular architecture of carbon nanotubes.[4,8−10] Further, advances in the separation of metallic and semiconducting tubes, as well as tubes with different diameters, were made.[11−16]

Unfortunately, it is difficult to fully characterize a given (heterogeneous) sample of carbon nanotubes. The length and diameter of an individual tube may be determined by atomic force microscopy (AFM), scanning tunneling microscopy (STM), or transmission electron microscopy (TEM) techniques. Information about a bulk sample may be obtained from scanning electron microscopy (SEM), X-ray diffraction, optical absorption, or Raman scattering. However, it appears that even a combination of these techniques does not fully characterize a given sample.[2]

One of the most versatile experimental tools to study the geometry and electronic structure of molecules and solids is nuclear magnetic resonance (NMR). Presently, it is fair to state that the full power of NMR for the characterization of nanotube samples has not yet been unleashed. Previous theoretical work proposed that metallic and semiconducting single-walled carbon nanotubes (SWNTs) should be clearly distinguishable by ^{13}C NMR because of a predicted 11−12 ppm difference in their chemical shifts.[17,18] However, on the basis of the same calculations, it was argued that NMR might not be able to resolve further structural differences between SWNTs.[17] An absolute value for the chemical shift with respect to a frequently used NMR reference was not given in ref 17 because not all terms that contribute to the nuclear magnetic shielding constant were calculated. Two of us have recently theoretically estimated the ^{13}C chemical shift of the (9,0) single-walled nanotube (SWNT) to be around 130 ppm (NMR reference: tetramethylsilane (TMS)). From a consideration of various approximations in the density functional theory (DFT) calculations of capped finite-size SWNT fragments, the value of 130 ppm was considered to be an upper bound with an estimated error of up to 5 ppm. On the basis of the theoretical results by Latil et al.,[17] one might expect a weak dependence of the shift on diameter and helicity. Consequently, by adding the predicted 11 ppm difference between semiconducting and metallic tubes from ref 17 we

* To whom correspondence should be addressed. E-mail: jochena@buffalo.edu.

10.1021/jp064540f CCC: $33.50
Published on Web 10/07/2006 PAGE EST: 9.8

estimated a shift of about 141 ppm for metallic tubes (provided a heterogeneous sample should exhibit NMR signals from semiconducting SWNTs below about 130 ppm similar to our results for the (9,0) system).

MAS-NMR measurements have indicated isotropic shifts of 124,[19] 116,[20] and 126 ppm for heterogeneous nanotube samples with side-bands ranging over 300 ppm.[18,21] The composition of the samples was not determined. Recently, experimental data have been reported by Kitaygorodskiy et al.[22] who were able to measure the ^{13}C chemical shift of poly(ethylene glycol) (PEG)-functionalized carbon nanotubes in solution after performing a rigorous purification process. A broad signal exhibiting a shoulder was deconvoluted into two peaks: one larger peak centered around 128 ppm and a smaller one centered around 144 ppm with an area ratio of about 1.8. On the basis of the availability of the theoretical estimates, the two broad signals were tentatively assigned to semiconducting (128 ppm) and metallic tubes (144 ppm). The breadth of the individual peaks was attributed to the presence of tubes with differing diameters and helicities. A solid-state MAS spectrum of a sample of functionalized nanotubes yielded a double peak (128 and 136 ppm) instead, with the same tentative assignment. Similar results were reported earlier in ref 18 from the deconvolution of a broad NMR signal for a nanotube sample based on T_1 relaxation time measurements. Metallic SWNTs were assigned the larger chemical shift, and a chemical shift difference of about 10 ppm was estimated. It is yet unclear how strong the influence of the functional groups on the ^{13}C chemical shifts of the tubes in solution might be. A recent NMR study on the protonation of SWNTs yielded a single broad solid-state MAS-NMR peak centered at 121 ppm instead, which was assigned to the pristine unprotonated SWNTs.[23] Comparison with the results of ref 22 suggests that the samples in the two studies might have had a different diameter distribution or a different ratio of metallic to semiconducting SWNTs. It is also conceivable that the chemical shifts in ref 22 might have been influenced by the functionalization or by solvent effects. Given the resolution that can nowadays be achieved in solution NMR measurements, one might expect that experiments using samples with an even higher degree of purification will eventually yield NMR spectra which exhibit a clearly visible structure due to the presence of the different SWNT structures.

Hence, it is important to determine theoretically from first principles what differences to expect for the chemical shift of SWNTs with different diameters and helicities. The knowledge of these differences will allow estimation of the experimental resolution necessary for the characterization of a nanotube sample by NMR. Further, the question arises of whether differing lengths of nanotubes manifest themselves in noticeable differences of the NMR chemical shift. For an analysis of an NMR spectrum with the help of calculated data, it is vital to determine the chemical shift range of SWNTs, and to study the error bars of the computational approach and the resulting dependence of predicted chemical shifts on the choice of the reference. Two related theoretical studies have appeared recently. One of them focused on the NMR of a range of infinite (n,0) SWNTs with mod(n,3) $\neq 0$ which were studied by DFT.[24] Unfortunately, ref 24 did not report results for the (9,0) system for comparison. Otherwise, the results confirmed the expectation that significant differences in the chemical shift of SWNTs will only be seen for small-to-medium-diameter systems because the vanishing curvature of the larger-diameter tubes must ultimately lead to a convergence of their properties to those of a single graphene sheet. However, the authors concluded that with better samples NMR might indeed become a key tool to characterize nanotubes. In another theoretical study, Hartree−Fock results for various finite tubes capped with fullerene hemispheres were presented.[25] The Hartree−Fock data of ref 25 do not take electron correlation into account. Because chemical shift calculations can potentially involve a large amount of error cancellation between the shielding constant of the probe and the reference, the Hartree−Fock results might be comparable to more accurate correlated methods. If this is really the case for SWNTs of varying diameters is yet unclear. Another limitation has been the finite size of the systems and small basis sets. The conclusions from our previous calculations were also limited in the sense that isolated finite-sized capped SWNT fragments for a single (9,0) tube were studied with a molecular DFT NMR program. For example, it is not yet clear whether the chemical shifts and other properties of finite SWNTs of different diameters converge to the infinite-length limit at the same rate.

In the present work, we extend upon this finite-length approach and present DFT calculations of infinite small-to-medium-diameter (n,0) SWNTs in order to obtain theoretical estimates for the chemical shift range of semiconducting carbon nanotubes. The calculations were performed with a gauge-including projector-augmented plane-wave (GIPAW) basis using periodic boundary conditions. Further, results for the infinite (9,0) tube, a finite (9,0) SWNT fragment, and two molecules (benzene and C_{60}) that were obtained with the GIPAW method are compared to molecular gauge-including atomic orbital (GIAO) calculations in order to assess the influence of finite tube length and of various other approximations, and to determine a suitable choice of the NMR reference in the computations. The effect of intertube interactions is also investigated by studying the energy and NMR chemical shifts of the (7,0) and (9,0) systems as a function of the intertube distance. Our results yield a shift range of about 20 ppm for $n = 7-17$ and suggest that NMR might become a useful tool for the characterization of SWNT samples.

Section II is concerned with details of the computations. We briefly investigate structural parameters and report the calculated band gap of the (n,0) systems where $n = 7-17$ (section IIIA). Calculated NMR chemical shifts for infinite SWNTs are presented and discussed in sections IIIB−D. Our findings are summarized in section IV. The Appendix presents a detailed study on the choice of the NMR reference. In particular, we show that it is indeed possible to directly compare values from periodic and molecular calculations if benzene is chosen as the computational reference.

II. Methodology, Computational Details

Electronic structure computations on infinite (n,0) SWNTs, with $n = 7-17$, were performed with a 2005 developer's version of the CASTEP code.[26] NMR shielding tensors for infinite SWNTs were computed with the same code using the gauge-including projector-augmented plane-wave (GIPAW) method implemented by Pickard and Mauri[27] and extended to ultrasoft pseudopotentials.[28,29] In the calculations, we have applied the Perdew−Burke−Ernzerhof (PBE) as well as the revised PBE (RPBE) nonhybrid gradient density functionals[30−33] and the Vosko−Wilk−Nusair[34] (VWN) local density approximation (LDA). For the calculations on isolated nanotubes (see below), a "precise" setting for the plane-wave basis with the ultrasoft pseudopotential resulted in an energy cutoff of about 420 eV. Test calculations were performed to ensure that energies, geometries, and nuclear shielding constants were sufficiently converged using this energy cutoff. For a number of test systems,

we determined that the nuclear shielding constants changed from a "fine" (cutoff: 350 eV) to a "precise" (420 eV) setting by less than 1 ppm. Among those test systems, for the rather sensitive (9,0) SWNT, changing the cutoff further from 420 to 500 eV changed the shielding by less than 0.2 ppm. We consider this to be an acceptable error compared to other approximations made in the calculations. The macroscopic component $\sigma(\mathbf{G} = 0)$ of the isotropic nuclear magnetic shielding has been determined as $-(4\pi/3)\sum_i \alpha_{ii}\chi$, with χ being the macroscopic magnetic susceptibility.[35] The α_{ii} were assigned values of $^2/_3$ uniformly, corresponding to a spherical shape of the macroscopic system. Geometry optimizations of nanotubes were performed on the basis of the initial structures generated by the TUBEGEN tool[36] using a hexagonal unit cell. Isolated SWNTs were simulated in the calculations by using an intertube distance of 8 Å. Full geometry optimizations (all internal coordinates as well as all cell parameters) were performed for these systems, leading to negligible changes of the cell parameters. This demonstrates that intertube interactions are insignificant at this distance. For the (7,0) and (9,0) systems, we have studied the dependence of binding energy and NMR chemical shifts on the intertube distance. For these systems, constrained optimizations were performed at fixed intertube distances by freezing the cell parameters $a = b$ and optimizing all other coordinates.

A Monkhorst−Pack k-point grid of dimension (1, 1, m) has been used for the "isolated" SWNTs where m was determined to ensure convergence of the total energy, forces, and shielding constants with acceptable numerical precision. We have used $m = 25$, 20, 25, 20, 35, 25, 30, and 25 for the (7,0), (8,0), (10,0), (11,0), (13,0), (14,0), (16,0), and (17,0) tubes, respectively. For these systems, the chemical shifts obtained for the k-grid reported here yielded average nuclear magnetic shielding constants that are converged to within 0.01 ppm compared to calculations with larger m (PBE functional). For the isolated (7,0) and (8,0) SWNTs, we have additionally compared results from calculations with (1, 1, 10) and (2, 2, 10) k-grids, with negligible differences. For the influence of the size of the k-grid in the $a^* = b^*$ direction for SWNTs with smaller intertube separations, we refer to the discussion in section IIID.

The small-gap semiconducting (n,0) SWNTs with $n = 9$, 12, and 15 required larger k-grids. For instance, for the (9,0) system, the shielding with $m = 40$ differed by about 2 ppm from the shielding calculated with $m = 35$. For the (12,0) SWNT, calculations with larger grids of $m = 76$ (excluding the Γ point) and $m = 77$ (grid includes Γ) were also not converged but yielded shielding constants that still differed by about 6 ppm. Calculations with even and odd m were found to converge smoothly but very slowly to the same value from opposite directions such that alternating even and odd m yielded alternating NMR shieldings; see Figure 1. The average of the two series converges much faster. We assume that this average, if converged, might be used as an estimate for the chemical shift of a fully converged calculation which we were not able to obtain because of computational limitations. For the (9,0) system, we found a similar but less strongly oscillating convergence behavior which is also illustrated in Figure 1 in comparison to the fast convergence for the (8,0) SWNT. As one might expect, for the (15,0) SWNT which belongs to the same family as (9,0) and (12,0) but has a smaller band gap, a similar but even more strongly oscillatory convergence behavior is found. Our reported chemical shift for this system is obtained from the average of shielding constants calculated with $m = 95$ and $m = 100$. With limited computational resources at hand, the average chemical shift of the odd and even k-grid series

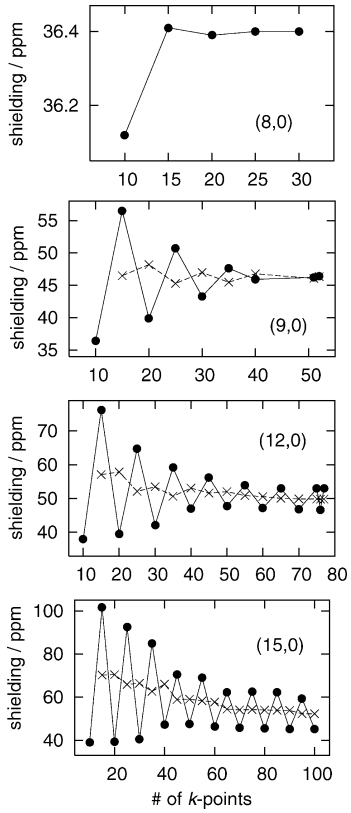

Figure 1. Convergence of the nuclear magnetic shielding constant for isolated (n,0) SWNTs with $n = 8$, 9, 12, and 15 as a function of the number of k-points in the c^* direction. Filled circles, calculated shielding constant; crosses, average of the shielding calculated with a given k-grid and the next smaller one. Lines were added to guide the eye.

reported later should be considered with an uncertainly of several ppm, although we found that the results for the (15,0) system fit rather well with the trend that we obtained from the (9,0) and (12,0) data (see section IIIB). In order to explain the nature of the oscillatory convergence behavior of the nuclear shieldings for the (9,0), (12,0), and (15,0) tubes, we have examined the convergence of the total energies, as well as that of the band gap, with an increasing number of k-points. The total energies converged exactly in the same manner as the shieldings (i.e., for even and odd m, they exhibited minima and maxima, respectively), with remaining oscillations of the total energy of meV magnitude for the largest k-grids used here. The band gaps displayed the opposite behavior (maxima for even and minima for odd m), and the convergence was not as regular. Thus, there is an oscillatory behavior in the electronic structure depending on the k-grid that becomes amplified in the shieldings. This is not too surprising, since the nuclear shielding is known to be very sensitive to changes in the electronic structure.

GIPAW calculations on the molecules TMS, benzene, and C_{60} have been performed using cubic supercells of size 10, 10, and 15 Å and k-grids of (2, 2, 2), (1, 1, 1), and (1, 1, 1), respectively. The plane-wave cutoffs corresponded to 490, 490, and 420 eV for the aforementioned molecules. By comparison of the results for different cell sizes, we have found that the effect of intermolecular interactions on the energy and the NMR shielding constants can be neglected for supercells of this size. The k-grids were also checked for convergence. Additionally, a calculation on a capped finite nanotube fragment with 150 atoms was performed using a supercell of dimensions (15, 15, 25) Å, a plane-wave cutoff of 420 eV, and one k-point. All

TABLE 1: Calculated Band Gaps for the (*n*,0) SWNTs Studied in This Work, in eV (PBE Functional)

n	calcd	scaled[a]	other DFT[b]	exptl[c]
7	0.200	0.240	0.19	
8	0.579	0.694	0.73	
9	0.096	0.115	0.20	0.080
10	0.761	0.913	0.88	1.1
11	0.912	1.094	1.13	
12	0.046	0.055	0.08	0.042
13	0.629	0.754	0.73	
14	0.701	0.841	0.90	
15	0.025	0.030	0.14	0.029
16	0.531	0.638	0.61	
17	0.575	0.690		

[a] Calculated values multiplied by a scaling factor of 1.20 to aid comparison with ref 39. [b] Scaled DFT band gaps from ref 39 (PW91 functional). [c] Experimental data for $n = 9$, 12, and 15 taken from ref 40. Experimental data for $n = 10$ from ref 41.

calculations were based on optimized geometries obtained with the same computational settings.

In addition to the GIPAW calculations with the CASTEP code, we have performed DFT NMR calculations on isolated molecules using Slater-type gauge-including atomic orbital (GIAO) basis sets as implemented in the Amsterdam Density Functional (ADF) code.[37] The computational settings were the same as in our previous study of (9,0) SWNT fragments. For further details, we refer to ref 38.

All chemical shifts for the infinite systems will be reported as average values for all atoms in the unit cell. It should be noted that the calculated shifts for different atoms in the unit cell differed by an amount less than the estimated error bars due to *k*-grid and plane-wave cutoff and residual intertube effects.

III. Results and Discussion

A. Structural Parameters and Band Gaps. Optimized structures and band gaps from DFT calculations have been published recently by Kertesz et al.[39] for a variety of SWNTs. In Table 1, we compare the calculated band gaps obtained here with the PBE functional to the results of ref 39 as well as some available experimental data. It has been noted previously in ref 39 that the band gaps calculated with nonhybrid DFT have a tendency to be too small compared with those obtained from experiment, which is an expected outcome of this type of DFT calculations. Therefore, a scaling factor of 1.20 has been applied in ref 39, and for comparison also in Table 1. As can be seen from Table 1, the scaled PBE results are in reasonable agreement with the DFT data of ref 39 (PW91 functional) but are closer to experiment. For the (9,0) and (12,0) tubes, the unscaled PBE results are in better agreement with experiment than the scaled ones. For the (15,0) tube, on the other hand, the scaled result is only slightly better. The different electronic character of the (*n*,0) SWNTs becomes obvious from the magnitude of the band gaps. The very small value of 0.046 eV (unscaled) for the (12,0) system is reflected in the previously discussed difficulties to obtain a converged nuclear magnetic shielding constant with respect to the size of the *k*-grid. Originally, (n_1,n_2) tubes with $\lambda = \mathrm{mod}(n_1 - n_2, 3) = 0$ were thought to be metallic,[42,43] but when s−p hybridization is considered the small-diameter members of this series were found to be small-band-gap semiconductors.[42−44] The much smaller band gaps of these SWNTs, exemplified by the $\lambda = 0$ family [(9,0), (12,0), and (15,0)] in our calculations, demands a significantly larger grid in *k*-space to obtain converged NMR parameters as compared to systems with $\lambda \neq 0$. The structural parameters (bond lengths and angles) for SWNTs calculated for the present work were found to be in agreement with those published previously.[39]

TABLE 2: Calculated Chemical Shifts of SWNTs (Infinite Systems Unless Noted Otherwise)

n	PBE[a]	RPBE[a]	PBE[b]	RPBE[b]	other Calc.
7	147.3	145.9	136.2	136.4	
8	141.5	140.3	130.4	130.8	131.5[c]
9	131.6	130.4	120.5	120.9	130.1,[d,e] 130[d,f]
10	137.7	136.4	126.6	126.9	129.5,[c] 130.3[d,e]
11	134.6	133.5	123.5	124.0	127[c]
12	128.1	126.4	117.0	116.8	
13	133.3	132.1	122.2	122.6	126.5[c]
14	131.2	130.0	120.1	120.5	124.8[c]
15	125.6	124.2	114.5	114.7	
16	130.9	129.6	119.8	120.1	124.5[c]
17	129.1	127.9	118.0	118.4	124[c]

[a] Present work, using the GIPAW CASTEP code and TMS as the NMR reference (i.e., $\delta^{\mathrm{TMS}}_{\mathrm{TMS}}$). [b] Same as footnote *a* but calculated with benzene as the internal NMR reference (i.e. $\delta^{\mathrm{TMS}}_{\mathrm{C_6H_6}}$). The difference with footnote *a* is 11.1 ppm for the PBE functional and 9.55 ppm for the RPBE functional. See text for details. [c] GIPAW calculations with the PBE functional, ref 24. Internal NMR reference: benzene. [d] Calculations performed on finite capped tubes. [e] Hartree−Fock calculations, ref 25. Reference: TMS. [f] TZP/revPBE, ref 38. Reference: TMS.

B. NMR Chemical Shifts of Isolated Infinite SWNTs and Comparison with Data for Finite SWNT Fragments. Table 2 lists the calculated NMR chemical shifts for isolated SWNTs obtained in this work. Available data from the literature for finite- and infinite-length SWNTs are also collected for comparison. As shown in the Appendix, using benzene or C_{60} as the internal (computational) reference, instead of TMS, results in fortuitous error cancellation and yields chemical shifts which should be closer to those measured experimentally. We have applied the PBE and the RPBE functionals and used TMS ($\delta^{\mathrm{TMS}}_{\mathrm{TMS}}$) and benzene ($\delta^{\mathrm{TMS}}_{\mathrm{C_6H_6}}$) as the NMR references with

$$\delta^{\mathrm{TMS}}_{\mathrm{TMS}}(\mathrm{tube}) = \sigma(\mathrm{TMS}) - \sigma(\mathrm{tube}) \quad (1)$$

$$\delta^{\mathrm{TMS}}_{\mathrm{C_6H_6}}(\mathrm{tube}) = \{\sigma(\mathrm{C_6H_6}) - \sigma(\mathrm{tube})\} + \delta^{\mathrm{TMS}}_{\mathrm{TMS}}(\mathrm{C_6H_6}) \quad (2)$$

where the shielding constants σ were computed and $\delta^{\mathrm{TMS}}_{\mathrm{TMS}}(\mathrm{C_6H_6})$ is the experimental chemical shift for benzene. Thus, only TMS-referenced chemical shifts are reported even when benzene is used as the internal reference. Ideally, both chemical shifts should be identical. However, because the GIPAW calculations with the PBE functional underestimate the ^{13}C nuclear shielding of benzene by 11.1 ppm (see the Appendix), the $\delta^{\mathrm{TMS}}_{\mathrm{C_6H_6}}$ values are always 11.1 ppm smaller than $\delta^{\mathrm{TMS}}_{\mathrm{TMS}}$ for a given system and considered more accurate.

As was found recently by Marques et al. in ref 24, the chemical shifts δ of families of (*n*,0) SWNTs characterized by $\lambda = \mathrm{mod}(n,3)$ can be fitted well by the function

$$\delta/\mathrm{ppm} = A(\lambda)/D + B \quad (3)$$

where *D* is the tube's diameter, *B* is the chemical shift limit for infinite diameter, and $A(\lambda)$ is a constant that depends on the nanotube family. For the series with $\lambda = 1$ ($n = 7$, 10, 13, ...), the constant $A(\lambda)$ was found to be larger than that for $\lambda = 2$ ($n = 8$, 11, 14, ...). It was noted by Marques et al. that the fitted *B* value of 116 ppm obtained for both families was in reasonable agreement with an estimate of 128 ppm for a graphene sheet.[24] In theory, the NMR shifts of metallic and small-gap SWNTs should converge to the same (graphene) value as semiconducting SWNTs when approaching an infinite radius. Thus, it will be

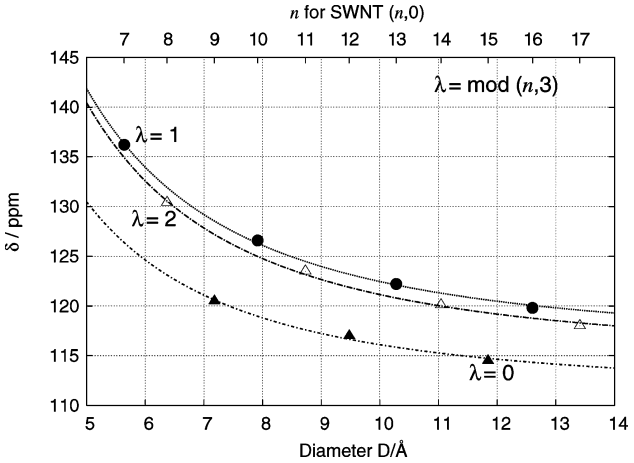

Figure 2. Calculated chemical shifts $\delta^{TMS}_{C_6H_6}$ of various SWNTs (PBE functional, column 4 of Table 2) as a function of the optimized tube diameter.

interesting to determine whether for metallic and small-gap large-diameter SWNTs the *B* parameters will actually be the same as those for larger-gap semiconducting SWNTs. For instance, on the basis of the 11 ppm larger chemical shift predicted for metallic SWNTs by Latil et al.,[17] a fit according to eq 3 should yield a difference of 11 ppm in the parameter *B*. Presently, we cannot study metallic systems with the GIPAW approach as implemented in the CASTEP code. However, herein, we present the first calculated chemical shifts of the small-gap semiconducting $\lambda = 0$ ($n = 9, 12, 15, ...$) series. We can see from our results in Table 2 that the chemical shifts in this family are significantly smaller than those for the other two families. We recall that the calculated band gaps are much smaller for the $\lambda = 0$ family. For a smaller band gap, we may expect a larger magnitude of the shielding constant due to the implicit occurrence of occupied-empty empty band energy difference denominators in the expression of the shielding tensor. Given that the shielding constants and chemical shifts for TMS, benzene, C_{60}, and SWNTs are positive, smaller band gaps should lead to smaller chemical shifts. The argument is of qualitative nature, of course, and does not account for differences in the matrix elements that enter the shielding tensor. The argument does not explain the trends among the $\lambda = 1$ and $\lambda = 2$ families for small diameters. For instance, the band gaps of the (7,0) and (8,0) SWNTs are smaller than those of the (10,0) and (11,0) SWNTs, respectively, but the chemical shifts of the (7,0) and (8,0) SWNTs are larger (compare Tables 1 and 2). We tentatively attribute this behavior to changes in the $s/p_\sigma/p_\pi$ mixing in the bands of the small-diameter SWNTS.

Fitting our calculated PBE chemical shifts to the optimized tube diameters according to eq 3, we obtain for $\delta^{TMS}_{C_6H_6}$

$$A(0) = 109(4)\ \text{Å};\ B(0) = 105.4(5) \quad (4a)$$

$$A(1) = 169(8)\ \text{Å};\ B(1) = 106(1) \quad (4b)$$

$$A(2) = 151(5)\ \text{Å};\ B(2) = 106.5(6) \quad (4c)$$

The *B* parameters for δ^{TMS}_{TMS} are 11.1 ppm larger. The fits are plotted along with the calculated shifts in Figure 2. As mentioned above, a fit of $\delta^{TMS}_{C_6H_6}$ in ref 24 for the $\lambda = 1$ and $\lambda = 2$ families yielded *B* parameters of 116.0 and smaller *A* parameters. A comparison of the data in Table 2 shows that the shifts for the (8,0) SWNT agree quite well, but for increasing tube diameter, the calculated chemical shifts for this work decrease faster than those of ref 24. The origin of the discrepancy is presently unclear, since the calculations differ in a number of aspects such as the pseudopotential, the size and symmetry of the supercell, and the treatment of the $\sigma(\mathbf{G} = 0)$ shielding component. It is interesting to note that the infinite-diameter limits *B* for all three families including the small-gap $\lambda = 0$ family agree within the standard deviations of the fits.

Our results suggest that in a SWNT sample that allows to resolve NMR signals within about 1 ppm one might be able to identify the medium-to-small-diameter systems. When comparing the shifts, we see that among the (*n*,0) SWNTs members of the $\lambda = 0$ family differ from the other two families by their significantly lower shift. However, it has to be determined how to distinguish these from the $\lambda = 1,2$ systems with large diameter. If the chemical shift range for SWNTs is predicted accurately by DFT calculations as performed here, it might be possible to predict the shapes and widths of NMR signals for different sample compositions computationally. In order to complete this task, future studies will need to investigate the chemical shifts of varying helical and metallic SWNTs. Regarding an extrapolation of the fits in eq 4, it is unclear whether the shifts of the $\lambda = 0$ tubes with $n \geq 18$ will adhere to the fit, since they will have almost vanishing band gaps. The shift range of the semiconducting SWNTs which we have specifically considered is about 20 ppm, with the $n = 7$, 8, and 10 species displaying the highest shifts. These tubes then have a shift which falls within the range expected for larger-radius metallic tubes, based upon the aforementioned calculations by Latil et al.[17] which predicted metallic tubes to have an 11 ppm higher chemical shift than semiconducting tubes. However, among other approximations that were applied in ref 17, the calculations neglected the Knight shift because of the vanishing density of states at the Fermi level. Recent work has indicated that ultranarrow zigzag nanotubes should exhibit a Knight shift which is on the order of hundreds of ppm, whereas tubes wider than 1.5 nm will have a Knight shift which is proportional to their diameter.[52] In contrast to the predicted shift of metallic SWNTs, the members of the small-band-gap $\lambda = 0$ family that we could study here have a chemical shift that is significantly lower than that of other semiconducting (*n*,0) SWNTs of similar diameter.

If we compare the literature data for the finite-size capped (9,0) SWNT, we note that the Hartree−Fock (HF) δ^{TMS}_{TMS} of ref 25 and our previous revPBE/TZP δ^{TMS}_{TMS} obtained for a 222-atom fragment are in good agreement. The agreement with the HF/STO-3G value might be accidental or indicate that with an AO basis of minimum flexibility a large amount of error cancellation is obtained at the HF level. As we have noted in the Appendix, $\delta^{TMS}_{C_6H_6}$ should yield better error compensation and we arrive at a revised chemical shift of 127 ppm for the 222-atom system. This is still 6.5 ppm higher than the calculated $\delta^{TMS}_{C_6H_6}$ for the infinite isolated (9,0) SWNT. In the Appendix, it is also shown that direct comparison between the molecular and periodic calculations should be possible if benzene is used as the internal reference. Most of the 6.5 ppm difference must therefore be attributed either to a very slow convergence of the NMR parameters of the finite-length systems irrespective of the capping or to capping effects that remain strong even for very extended finite systems, or a combination of both. From previous results, the shifts of the central carbon atom appeared to change very slowly with respect to the tube length, suggesting that the difference is mainly due to capping effects. In order to verify this, we have calculated $\delta^{TMS}_{C_6H_6}$ for the central carbon atom in a number of progressively longer finite (9,0) nanotubes with TZP/

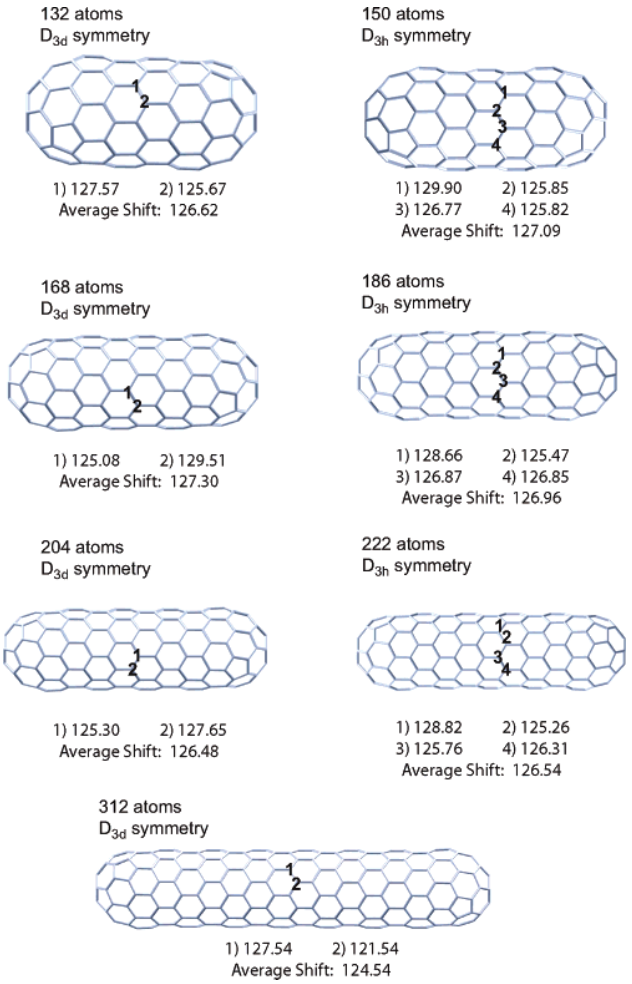

Figure 3. Calculated NMR chemical shifts $\delta^{TMS}_{C_6H_6}$ of the central carbon atoms in a number of finite, C_{30}-capped (9,0) SWNTs. The calculations were performed with the ADF code at the revPBE/TZP level of theory.

revPBE. For the present work, we have extended the size range to include a system with 312 carbon atoms and determined several additional chemical shifts for symmetry-inequivalent central atoms for the shorter 222- and 204-atom systems. These shifts were not determined in our previous SWNT study[38] due to the high computational expense. However, one of us (J.A.) has recently implemented speed-ups in the ADF NMR code that have made parallelized computations on large molecules feasible. (These improvements only affect the scaling of the algorithms with the size of the system in parallel computations, not the final results.)

Assuming that the difference in shifts will be the same as that for the 150-atom tube when benzene is used as the internal reference, the TZP/revPBE values should not differ by more than 0.5 ppm from ones calculated with TZP/PBE. The series with D_{3d} and D_{3h} symmetry yield two and four symmetry-inequivalent central atoms, respectively. The results in Figure 3 reveal that the average shift does not vary by more than 0.8 ppm from the 132-atom fragment (which has "little tube between the caps") and the 222-atom system studied previously. However, for a given tube, the individual shifts in the center vary considerably even for quite long systems. For the D_{3d} series, the shift is somewhat higher for a carbon atom which is directly linked to the vertex of a pentagonal face on the cap. No obvious trend correlating atomic position with the chemical shift for the D_{3h} series could be found. When including the 312-atom system in the data set, it can be seen that the shifts up to the 222-atom system are not converged and that the cap plays a significant role in all of these systems. The capping effects remain quite strong at the tube's center even for comparatively long tubes. In particular, the shifts of the central carbon atom for a given tube vary from about 2 ppm up to 6 ppm for the 312-atom SWNT. Moreover, the HOMO−LUMO gap was calculated as being 0.55 and 0.38 eV for the tubes containing 222 and 312 carbons, respectively, which indicates that the capping and the finite length of the tube should have a considerable influence on its magnetic properties even for these relatively large systems. It has been pointed out by some authors that it might not be possible to extrapolate the properties of infinite systems from cluster-type calculations in a straightforward way,[53] implying that the shifts of the central carbon atoms calculated for finite tubes might not converge smoothly to those obtained for infinite ones. Recently, a number of studies have appeared which study how fullerene hemispheres influence the geometry and vibrational structures of finite nanotubes.[47−49] These studies also indicated that the capping influences the properties of finite-length SWNTs quite significantly. Further studies on finite tubes should help to clarify if the chemical shift difference for the (9,0) system is an exception or the rule and to what size one needs to extend the GIAO calculations in order to obtain a result close to the GIPAW value obtained for the infinite system.

The Hartree−Fock δ^{TMS}_{TMS} for a finite (10,0) model system taken from ref 25 is only 0.2 ppm larger than the one for the (9,0) model system. Increasing the length of the model system yielded a decreasing chemical shift which suggests that the 130.3 ppm value quoted in Table 2 is an upper bound for the Hartree−Fock result. However, our calculations on the infinite systems yield a chemical shift for the (10,0) SWNT that is about 6 ppm larger than that of the (9,0) SWNT. It may be possible that the minimal basis used in ref 25 is not capable of describing the change in the polarization of the carbon atoms for different SWNT curvatures well enough; that is, the level of error compensation might not be systematic for tubes of different diameters. Another reason for the discrepancy might be that the convergence of the finite SWNT chemical shifts with tube length is very different for the different families or even for each individual (n,0) structure.

C. Shielding Tensor Orientation. The shielding tensor orientation for the infinite (9,0) system is shown in Figure 4. It is qualitatively the same as that obtained previously for finite (9,0) SWNT fragments:[38] a large diamagnetic (positive) principal component is perpendicular to the tube's surface (radial component, σ_{33}), while two paramagnetic (negative) components are parallel to the tube's surface (ortho-radial & axial or longitudinal). Relative to C_{60}, the smaller chemical shift in the SWNTs is due to a simultaneous increase of the magnitude of the positive σ_{33} component and a decrease of the magnitude of the negative σ_{11} and σ_{22} components. The C_{60} tensor orientation calculated with the same plane-wave approach is also shown in Figure 4. For a comparison between the $l = 0$ SWNT and the other (n,0) SWNTs, Figure 4 further displays the shielding tensor orientation for the (8,0) system. Here, we find two relatively large negative principal components and a smaller radial component than that for the (9,0) system. The larger chemical shift (smaller shielding) of the (8,0) SWNT as compared to the (9,0) SWNT is due to the fact that the increase in the radial principal component is overpowered by an increased magnitude of the negative axial component. The work by Latil et al.[17] predicted that the shielding tensor of metallic and semiconducting SWNTs should differ mainly in the axial principal component. Because of neglected terms in the shielding

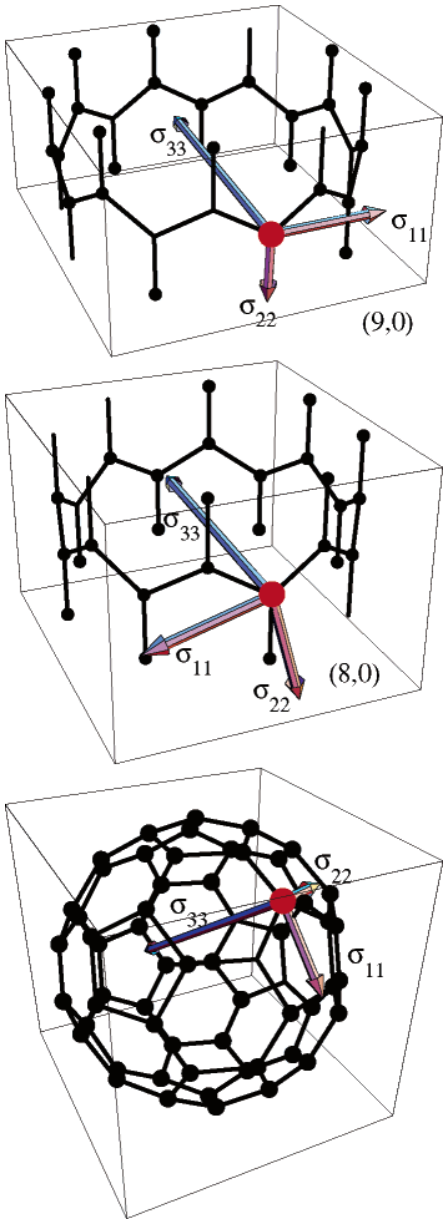

Figure 4. (top) Orientation of the shielding tensor for the infinite (9,0) SWNT. The arrows indicate the principal axes. The arrows' lengths reflect the magnitude of the principal shielding components. For reasons of clarity of presentation, they are not proportional. σ_{33} is large and positive, and the other two components are negative and an order of magnitude smaller. For a GIPAW calculation with the PBE functional and 40 *k*-points, the principal components were $\sigma_{11} = -25.9$, $\sigma_{22} = -3.2$, and $\sigma_{33} = +166.8$ ppm. (middle) Tensor orientation for the (8,0) SWNT. PBE functional, 20 *k*-points. $\sigma_{11} = -32.2$, $\sigma_{22} = -29.2$, and $\sigma_{33} = +170.4$ ppm. (bottom) Tensor orientation for C_{60} calculated with the same plane-wave method. $\sigma_{11} = -42.7$, $\sigma_{22} = -17.0$, and $\sigma_{33} = +131.4$ ppm.

tensor, Latil et al.'s calculations further yielded negative isotropic shielding constants for the metallic SWNTs, whereas the shielding constants of the semiconducting SWNTs are positive in both ours and Latil et al.'s work. In a comparison of the (8,0) SWNT with the small-gap (9,0) SWNT, we find that the axial principal components of the shielding tensors differ significantly. The differences in the radial and ortho-radial components are certainly not negligible but roughly an order of magnitude smaller. The small-gap $\lambda = 0$ family does not appear to behave "more metallic" than the SWNTs with larger band gaps in the sense that they have smaller chemical shifts,

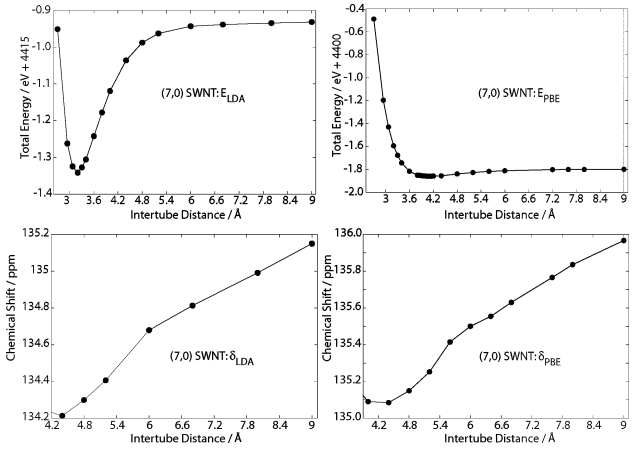

Figure 5. Energy and chemical shift $\delta^{\mathrm{TMS}}_{C_6H_6}$ of the (7,0) SWNT as a function of intertube distance.

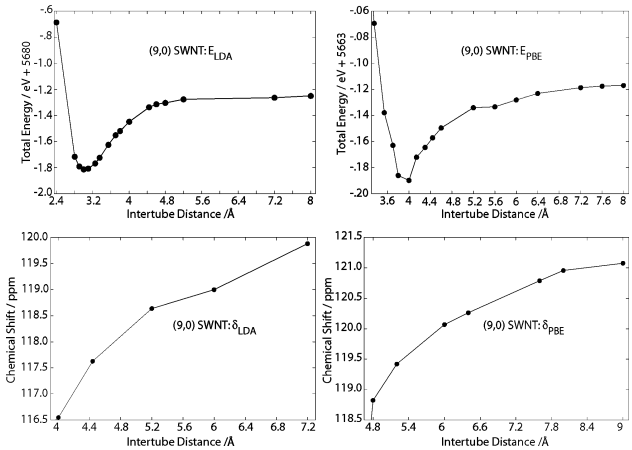

Figure 6. Energy and chemical shift $\delta^{\mathrm{TMS}}_{C_6H_6}$ of the (9,0) SWNT as a function of intertube distance.

whereas the calculations of ref 17 predicted metallic SWNTs to have a larger chemical shift. Clearly, the chemical shift difference between metallic and semiconducting SWNTs needs further investigation.

D. Intertube Distance Dependence of Energies and NMR Chemical Shifts for the (7,0) and (9,0) SWNTs. The main purpose of this work has been to study the NMR of isolated SWNTs. In order to investigate a possible effect from interactions between SWNT images in the GIPAW calculations, we have studied the dependence of the chemical shift on the intertube distance for the (7,0) and (9,0) systems. Further, we were interested in the location and depth of the potential energy minimum. Constrained optimizations were performed for this purpose where the $a = b$ cell parameters were kept fixed but all other geometrical parameters were optimized. For distances larger than 4.5 Å, a (1, 1, *m*) grid was found to be sufficient, whereas, for smaller intertube separations (2, 2, *m*) and (3, 3, *m*), grids were necessary to obtain converged energies. The results are displayed in Figures 5 and 6 for the (7,0) and (9,0) SWNTs, respectively.

The potential energy curves are strongly dependent upon the density functional that was chosen in the calculation. For the (7,0) SWNT, the LDA minimum is found around 3 Å. A very shallow PBE minimum is located at a significantly larger intertube distance, around 4 Å. In the range of 3 Å, the PBE potential is repulsive. For the (9,0) SWNT, the LDA minimum is also close to 3 Å, and again, there is virtually no binding at the PBE level of theory. For molecules, it is known that density-

gradient-dependent functionals such as PBE tend to overestimate bond distances but yield fairly reliable binding energies. LDA functionals, on the other hand, usually yield bond distances close to experiment but strongly overbind.[50] It can be seen that the discrepancies between LDA and gradient-corrected functionals are amplified for the comparatively weak nanotube−nanotube interactions which can be considered as a combination of short-range overlap and long-range van der Waals effects. The latter are not described by either functional. Our results are in agreement with recent findings regarding the capability of the LDA and PBE functional for describing the interlayer binding energy in graphite.[51]

Regarding the chemical shifts, it can be seen that for intertube distances of 5 Å and larger the chemical shifts undergo small but not negligible changes. Therefore, it appears that comparatively large intertube distances are needed for obtaining convergence of the shifts within a few tenths of a ppm. We believe that for the purpose of the present paper, where we have other sources of error that may easily exceed 0.1 ppm, an intertube distance of 8 Å represents a good compromise between the need for well-converged results and the associated computational expense.

IV. Conclusions

Previous work has estimated that the difference in the chemical shifts between semiconducting and metallic SWNTs is approximately 11 ppm.[17] Marques et al. have obtained a shift range of about 10 ppm for a number of semiconducting zigzag SWNTs of the $\lambda = 1$ and $\lambda = 2$ families with n between 8 and 20.[24] Our present work on semiconducting zigzag SWNTs including the $\lambda = 0$ family has resulted in a chemical shift range for (n,0) SWNTs with $n = 7-17$ of about 20 ppm. Our results indicate that, with highly purified samples that would allow for a higher resolution than what has been attained so far, NMR spectroscopy might become a very useful tool for the structural characterization of nanotube samples. Moreover, for all three sets of families, the chemical shift was found to decrease roughly inversely proportional to the tube's diameter.

In our calculations, the $\lambda = 0$ family of (n,0) SWNTs [(9,0), (12,0), (15,0), ...] exhibited significantly smaller NMR chemical shifts (larger nuclear magnetic shielding) than the $\lambda = 1$ and $\lambda = 2$ families. For these systems, we have reported the average of shifts calculated with large even and odd numbers of k-points, respectively. A fit to eq 3 yielded the same infinite-diameter limit for all three families of semiconducting zigzag SWNTs.

Given the magnitude of the chemical shift range of SWNTs, an uncertainty of 10 ppm for the calculated shift of semiconducting tubes would render the calculations rather useless for a confident prediction or assignment of experimental data. However, we have shown here that the calculations can afford errors of this magnitude unless a suitable NMR reference is chosen or because of additional error compensation, for example, from truncating the AO basis sets. For instance, although $\delta^{TMS}_{C_6H_6}(C_{60})$ agrees very well with experiment at the PBE/PW level, δ^{TMS}_{TMS} for benzene and C_{60} are about 11 ppm off. We believe that we have provided sufficient computational evidence to make the $\delta^{TMS}_{C_6H_6}$ results sufficiently trustworthy for calculations of NMR chemical shifts of carbon nanotubes. However, unless more accurate computational models become feasible for infinite SWNTs, a possible error of one to two ppm should be taken into consideration when comparing directly with experiment. It is not yet clear if the desired error compensation in $\delta^{TMS}_{C_6H_6}$ will be the same for all SWNTs of different diameters and helicities.

By using benzene or C_{60} as the NMR reference in the computations, it seems possible to calculate chemical shifts that are transferable between different computational models including "molecular" AO-basis computations on finite-size SWNT fragments. Regarding the latter, NMR calculations on model systems for the (9,0) SWNT show a comparatively large influence from the capping, leading to several ppm difference in the $\delta^{TMS}_{C_6H_6}$ chemical shifts between finite systems containing up to 312 atoms and the infinite system. It is not yet clear whether the convergence of the chemical shift in finite SWNTs with increasing tube length is similar for different SWNT structures. We plan to investigate this issue as well as potential influences on the NMR chemical shifts from the SWNT's helicity, polar functional groups, and defects.

Acknowledgment. J.A. acknowledges support from the Center of Computational Research at SUNY Buffalo and is grateful for financial support from the ACS Petroleum Research Fund (Grant No. 40987-G3) and from the CAREER program of the National Science Foundation (Grant No. CHE-0447321). E.Z. acknowledges financial support from the "International Max-Planck Research School for Advanced Materials" (IMPRS-AM). C.J.P. is supported by an EPSRC Advanced Research Fellowship.

V. Appendix

A. Choice of the NMR Reference. Experimentally, ^{13}C chemical shifts are usually reported with respect to tetramethylsilane (TMS). It is well-known that computations of chemical shifts can take advantage of a large amount of error cancellation due to an electronic similarity between the probe and the NMR reference. If we were able to perform exact calculations, the choice of the reference would obviously be irrelevant. However, in approximate calculations, a particular choice of the reference might or might not lead to large deviations between theory and experiment. To complicate matters, nuclear magnetic shielding constants are also strongly basis set dependent. Therefore, a convenient choice of a reference for calculations at a particular level of basis set flexibility might not perform as well if the quality of the basis is increased or decreased. The plane-wave basis sets employed in the GIPAW calculations can be regarded as being close to the basis set limit for valence shells, but this is certainly not the case for the GIAO basis sets used in computations of finite-size SWNT fragments. On the other hand, the GIAO basis sets provide a very good description of the core shells and the core tails of the valence orbitals without resorting to a pseudopotential. We have previously defined δ^{TMS}_{TMS} and $\delta^{TMS}_{C_6H_6}$ in eqs 1 and 2 above. Moreover, $\delta^{TMS}_{C_{60}}$ can be defined by replacing benzene by C_{60} in eq 2. Thus, all of our reported shifts are referenced to TMS. If the computational model would predict the shielding constants exactly all δ values should be the same and equal to the experimental TMS-referenced shift.

TMS is a rather "well-behaved" molecule in DFT NMR calculations. The shielding constants obtained with different (non-hybrid) functionals at varying levels of basis set flexibility do not differ much.[46] Benzene, however, has a complicated electronic structure which results in significantly different nuclear shielding constants calculated at various levels of theory. See Table 3. For example, even shielding constants obtained with functionals within the PBE family can differ by several ppm. Other functionals (e.g., BP and PW91) lead to even stronger variations. Out of those that we have tested, the revised PBE functionals (RPBE and revPBE) yield the best agreement with experiment overall. Marques et al.[24] have used benzene as

TABLE 3: Calculated Nuclear Magnetic Shielding and NMR Chemical Shifts of Benzene

functional	basis[a]	shielding	shift[b]
revPBE	TZP	54.66	129.82
RPBE	TZP	55.33	129.26
PBE	TZP	52.60	131.61
PW91	TZP	51.47	132.17
BP86	TZP	44.87	137.72
revPBE	QZ4P	44.55	134.60
RPBE	QZ4P	44.88	134.04
PBE	QZ4P	43.05	135.60
PW91	QZ4P	42.21	137.20
BP86	QZ4P	36.96	142.75
PBE	PW	39.94	137.99
RPBE	PW	41.48	136.45

[a] TZP and QZ4P: AO basis calculations with the ADF code. PW: plane-wave basis set calculations with the CASTEP code. [b] With respect to TMS optimized and calculated at the same levels of theory (δ^{TMS}_{TMS}). The experimental shift is 126.9 ppm as quoted in ref 24.

TABLE 4: Calculated Nuclear Magnetic Shielding and NMR Chemical Shifts of C_{60} (See Also the Footnotes of Table 3)

functional	basis	shielding	shift[a]
revPBE	TZP	39.28	145.20
RPBE	TZP	39.83	144.76
PBE	TZP	37.57	146.64
PW91	TZP	36.25	147.39
BP86	TZP	30.58	152.01
revPBE	QZ4P	29.42	149.73
RPBE	QZ4P	29.61	149.30
PBE	QZ4P	28.45	150.21
PW91	QZ4P	27.06	152.35
BP86	QZ4P	22.93	156.78
PBE	PW	23.89	154.04
RPBE	PW	25.24	152.69

[a] δ^{TMS}_{TMS}. The experimental shift is 142.68 ppm.[45]

the NMR reference in their recent computational study of carbon nanotubes (PBE functional) because the chemical environment of the carbon nuclei in nanotubes is presumably much more similar to that of benzene than to TMS. Another possible choice for the reference might be C_{60} (Table 4).

When comparing the plane wave with "molecular" results obtained for finite-size tube fragments using atom-centered Slater-type or Gaussian-type atomic orbital (AO) basis functions, it is important to know which level of AO basis compares best with the plane-wave basis employed in this work. To this end, we have performed calculations of the chemical shift of benzene and C_{60} with different GIAO basis sets using the ADF code in addition to calculations performed with CASTEP. The results are collected in Tables 3 and 4. Previous calculations for benzene showed that its calculated chemical shift increases as the basis size increases.[46] It can be seen that the PBE shifts for benzene obtained with the plane-wave basis are even larger than those obtained with the high-accuracy QZ4P GIAO basis. The same is found for C_{60}. Obviously, the plane-wave basis applied here in the GIPAW calculations represents a very flexible basis in the valence region of the carbon atoms. We may thus order the basis set flexibility as TZP < QZ4P < PW.

However, the chemical shifts obtained with a highly flexible basis are in considerable deviation from experiment (up to 10 ppm and more). This illustrates that fortuitously good agreement of δ^{TMS}_{TMS} with experiment for benzene and C_{60} can be obtained by a compensation of errors due to the basis set truncation and from approximations in the density functional. We have previously noted this in ref 38 in the context of NMR calculations on finite SWNT fragments. If the deviations between revPBE/TZP and experimental δ^{TMS}_{TMS} for benzene and C_{60} are transferrable to nanotubes, our previous molecular revPBE/TZP calculations on (9,0) tube fragment should be reasonably accurate apart from finite-size and capping effects; i.e., δ^{TMS}_{TMS} might overestimate the (hypothetical) experimental shift of finite (9,0) fragments by about 3 ppm.

TABLE 5: Calculated NMR Chemical Shifts for the Finite 150-Atom Nanotube Shown in Figure 3

	atom 1	atom 2	atom 3	atom 4
δ^{TMS}_{TMS} (revPBE/TZP)[a]	134.12	130.02	130.76	129.87
δ^{TMS}_{TMS} (PBE/TZP)[b]	134.22	130.07	131.04	129.98
δ^{TMS}_{TMS} (PBE/PW)[b]	140.78	136.21	137.28	136.06
δ^{TMS}_{TMS} (PBE/PW)[c]	140.98	136.52	137.58	136.37
$\delta^{TMS}_{C_6H_6}$ (PBE/TZP)[b]	129.51	125.36	126.33	125.27
$\delta^{TMS}_{C_6H_6}$ (PBE/PW)[c]	129.89	125.43	126.49	125.28

[a] From ref 38. [b] Geometry optimized with the ADF code and PBE/TZP. [c] Geometry reoptimized with CASTEP and the PBE functional.

At the revPBE/TZP level, δ^{TMS}_{TMS}(benzene) is 2.9 ppm and $\delta^{TMS}_{TMS}(C_{60})$ is 2.5 ppm above the experimental value. If the shielding constants of different nanotubes afford similar errors, both benzene and C_{60} would be excellent computational references at this level of theory. By comparison, PBE/TZP overestimates δ^{TMS}_{TMS} by 4.7 and 4.0 ppm for benzene and C_{60}, respectively. For PBE/QZ4P, we obtain deviations of 8.7 and 7.5 ppm, respectively. The results show that by using a very flexible GIAO basis $\delta^{TMS}_{C_6H_6}(C_{60})$ is about 1 ppm below the experiment. The question of which of the two molecules would be the "better" NMR reference therefore yields to an uncertainty of the calculated SWNT chemical shifts of at least that magnitude. In comparison, in the GIPAW calculations, we obtain $\delta^{TMS}_{C_6H_6}(C_{60}) = 143.0$ ppm, just 0.3 ppm larger than the experimental result.

Since we do not know the experimental NMR shift for one of the individual SWNT structures, we cannot decide conclusively how much error compensation is really obtained at the various theoretical levels for SWNT chemical shifts by using benzene or C_{60} as the reference. The comparison of GIAO and GIPAW results for benzene and C_{60} strongly suggests that δ^{TMS}_{TMS}(SWNT) values are too large by 10 ppm or even more, whereas $\delta^{TMS}_{C_6H_6}$ and $\delta^{TMS}_{C_{60}}$ should be close to the correct results. To investigate this issue further, we may study if a nanotube structure is magnetically similar to benzene and/or C_{60} by comparing how the shielding constants change between the TZP and the PW basis.

To this end, we have performed GIPAW calculations with the CASTEP code on a capped 150-atom (9,0) nanotube fragment as shown in Figure 3. For this system, shown in Figure 3, we have previously obtained GIAO shielding constants for the atoms furthest away from the caps that were similar to the shielding of one of the central atoms in a 222-atom SWNT. Here, we consider an isolated 150-atom tube and compare GIPAW results obtained with a large supercell to the GIAO results. Due to the fact that the revPBE functional is not available in CASTEP, we have reoptimized the tube and calculated its NMR chemical shielding using the PBE functional and the TZP GIAO basis set. This same geometry and PBE functional was then used for the plane-wave NMR calculations. Moreover, the geometry was reoptimized with CASTEP and the shieldings for this structure were subsequently computed. The results in Table 5 show that changes in the NMR chemical shifts from a geometry reoptimization with the plane-wave code

were within 0.3 ppm of the results obtained for the TZP/PBE optimized geometry. We therefore believe that slight differences between the AO- and PW-basis geometries should not affect the comparison. We found that from TZP/PBE to PW/PBE for the central carbons δ_{TMS}^{TMS} increased consistently by an average of 6.5 ppm. This should be compared to an increase of 6.4 ppm for benzene and 7.4 ppm for C_{60}, respectively. Thus, $\delta_{C_6H_6}^{TMS}$ differed by an average of 0.16 ppm; see the last two rows of Table 5. This suggests that if benzene is used as an internal reference in both the molecular and periodic calculations then the NMR chemical shifts obtained via the two approaches are directly comparable. Hence, it is possible to directly compare the finite and infinite values obtained for the (9,0) SWNT and to determine the degree to which capping has an effect on the chemical shift.

Supporting Information Available: Optimized structures and energies for infinite isolated SWNTs as used here in the calculations for Table 2, optimized with CASTEP using the PBE functional; CASTEP structures and energies for TMS, benzene, C_{60}, and the 150-atom tube; and structures and energies for the finite (9,0) SWNT optimized with ADF using the revPBE functional and the TZP basis. This material is available free of charge via the Internet at http://pubs.acs.org.

References and Notes

(1) Iijima, S. *Nature* **1991**, *354*, 56−58.

(2) Minett, A.; Atkinson, K.; Roth, S. Carbon nanotubes. In *Handbook of porous solids*; Schüth, F., Sing, S. W., Weitkapmp, J., Eds.; Wiley-VCH: Weinheim, Germany, 2002.

(3) Yao, Z.; Postma, H. W. C.; Balents, L.; Dekker, C. *Nature* **1999**, *402*, 273−276.

(4) Zhou, O.; Shimoda, H.; Gao, B.; Oh, S.; Fleming, L.; Yue, G. *Acc. Chem. Res.* **2002**, *35*, 1045−1053.

(5) Baughman, R. H.; Cui, C.; Zakhidov, A. A.; Iqbal, Z.; Barisci, J. N.; Spinks, G. M.; Wallace, G. G.; Mazzoldi, A.; De Rossi, D.; Rinzler, A. G.; Jaschinski, O.; Roth, S.; Kertesz, M. *Science* **1999**, *284*, 1340−1344.

(6) Kim, Y.-H.; Choi, J.; Chang, K. J.; Tomanek, D. *Phys. Rev. B* **2003**, *68*, 125420-4.

(7) Gao, H.; Kong, Y.; Cui, D. *Nano Lett.* **2003**, *3*, 471−473.

(8) Yudasaka, M.; Komatsu, T.; Ichihashi, T.; Achiba, Y.; Iijima, S. *J. Phys. Chem. B* **1998**, *102*, 4892−4896.

(9) Zhang, M.; Yudasaka, M.; Iijima, S. *J. Phys. Chem. B* **2004**, *108*, 149−153.

(10) Bandow, S.; Asaka, S.; Saito, Y.; Rao, A. M.; Grigorian, L.; Richter, E.; Eklund, P. C. *Phys. Rev. Lett.* **1998**, *80*, 3779−3782.

(11) Krupke, R.; Hennrich, F. *Adv. Eng. Mater.* **2005**, *7*, 111−116.

(12) Seo, K.; Park, K. A.; Kim, C.; Han, S.; Kim, B.; Lee, Y. H. *J. Am. Chem. Soc.* **2005**, *127*, 15724−15729.

(13) Banerjee, S.; Hemraj-Benny, T.; Wong, S. S. *J. Nanosci. Nanotechnol.* **2005**, *5*, 841−855.

(14) Maeda, Y.; et al. *J. Am. Chem. Soc.* **2005**, *127*, 10287−10290.

(15) Zheng, M.; Jagota, A.; Strano, M. S.; Santos, A. P.; Barone, P.; Chou, S. G.; Diner, B. A.; Dresselhaus, M. S.; McLean, R. S.; Onoa, G. B.; Samsonidze, G. G.; Semke, E. D.; Usrey, M.; Walls, D. J. *Science* **2003**, *302*, 1545−1548.

(16) Krupke, R.; Hennrich, F.; v. Löhneysen, H.; Kappes, M. M. *Science* **2003**, *301*, 344−347.

(17) Latil, S.; Henrard, L.; Goze-Bac, C.; Bernier, P.; Rubio, A. *Phys. Rev. Lett.* **2001**, *86*, 3160−3163.

(18) Goze-Bac, C.; Latil, S.; Lauginie, P.; Jourdain, V.; Conard, J.; Duclaux, L.; Rubio, A.; Bernier, P. *Carbon* **2002**, *40*, 1825−1842.

(19) Tang, X.-P.; Kleinhammes, A.; Shimoda, H.; Fleming, L.; Bennoune, K. Y.; Shina, S.; Bower, C.; Zhou, O.; Wu, Y. *Science* **2000**, *288*, 492−494.

(20) Hayashi, S.; Hoshi, F.; Ishikura, T.; Yumura, M.; Ohshima, S. *Carbon* **2003**, *41*, 3047−3056.

(21) Goze Bac, C.; Latil, S.; Vaccarini, L.; Bernier, P.; Gaveau, P.; Tahir, S.; Micholet, V.; Aznar, R. *Phys. Rev. B* **2001**, *63*, 100302-4.

(22) Kitaygorodskiy, A.; Wang, W.; Xie, S.-Y.; Lin, Y.; Fernando, K. A. S.; Wang, X.; Qu, L.; Chen, B.; Sun, Y.-P. *J. Am. Chem. Soc.* **2005**, *127*, 7517−7520.

(23) Engtrakul, C.; Davis, M. F.; Gennett, T.; Dillon, A. C.; Jones, K. M.; Heben, M. J. *J. Am. Chem. Soc.* **2005**, *127*, 17548−17555.

(24) Marques, M. A. L.; d'Avezac, M.; Mauri, F. *Phys. Rev. B* **2006**, *73*, 125433.

(25) Besley, N. A.; Titman, J. J.; Wright, M. D. *J. Am. Chem. Soc.* **2005**, *127*, 17948−17953.

(26) Segall, M. D.; Lindan, P. J. D.; Probert, M. J.; Pickard, C. J.; Hasnip, S. J.; Payne, M. C. *J. Phys.: Condens. Matter* **2002**, *14*, 2717−2744.

(27) Pickard, C. J.; Mauri, F. *Phys. Rev. B* **2001**, *63*, 245101-13.

(28) Yates, J. First principles calculation of magnetic resonance. Thesis, University of Cambridge, 2003.

(29) Vanderbilt, D. *Phys. Rev. B: Condens. Matter* **1990**, *41*, 7892−7895.

(30) Perdew, J. P.; Burke, K.; Ernzerhof, M. *Phys. Rev. Lett.* **1996**, *77*, 3865−3868.

(31) Zhang, Y.; Yang, W. *Phys. Rev. Lett.* **1998**, *80*, 890.

(32) Perdew, J. P.; Burke, K.; Ernzerhof, M. *Phys. Rev. Lett.* **1998**, *80*, 891.

(33) Hammer, B.; Hansen, L. B.; Norskov, J. K. *Phys. Rev. B* **1999**, *59*, 7413−7421.

(34) Vosko, S. H.; Wilk, L.; Nusair, M. *Can. J. Phys.* **1980**, *58*, 1200−1211.

(35) Mauri, F.; Pfrommer, B. G.; Louie, S. G. *Phys. Rev. Lett.* **1996**, *77*, 5300−5303.

(36) Frey, J. T.; Doren, D. J. "TubeGen 3.3 (web-interface, http://turin.nss.udel.edu/research/tubegenonline.html)", University of Delaware, Newark, DE, 2005.

(37) Baerends, E. J.; et al. "Amsterdam Density Functional, Theoretical Chemistry, Vrije Universiteit, Amsterdam", URL http://www.scm.com.

(38) Zurek, E.; Autschbach, J. *J. Am. Chem. Soc.* **2004**, *126*, 13079−13088.

(39) Sun, G.; Kürti, J.; Kertesz, M.; Baughman, R. H. *J. Phys. Chem. B* **2003**, *107*, 6924−6931.

(40) Ouyang, M.; Huang, J.-L.; Cheung, C. L.; Lieber, C. M. *Science* **2001**, *292*, 702−705.

(41) Odom, T. W.; Huang, J.-L.; Kim, P.; Lieber, C. M. *J. Phys. Chem. B* **2000**, *104*, 2794−2809.

(42) White, C. T.; Robertson, D. H.; Mintmire, J. W. *Phys. Rev. B* **1993**, *47*, 5485−5488.

(43) Saito, R.; Fujita, M.; Dresselhaus, G.; Dresselhaus, M. S. *Phys. Rev. B* **1992**, *46*, 1804−1811.

(44) Hamada, N.; Sawada, S.; Oshiyama, A. *Phys. Rev. Lett.* **1992**, *68*, 1579−1581.

(45) Taylor, R.; Hare, J. P.; Abdul-Sada, A. K.; Kroto, H. W. *J. Chem. Soc., Chem. Commun.* **1990**, *20*, 1423−1424.

(46) Le Guennic, B.; Neugebauer, J.; Reiher, M.; Autschbach, J. *Chem.—Eur. J.* **2005**, *11*, 1677−1686.

(47) Yumura, T.; Hirahara, K.; Bandow, S.; Yoshizawa, K.; Iijima, S. *Chem. Phys. Lett.* **2004**, *386*, 38−43.

(48) Yumura, T.; Bandow, S.; Yoshizawa, K.; Iijima, S. *J. Phys. Chem. B* **2004**, *108*, 11426−11434.

(49) Yumura, T.; Nozaki, D.; Bandow, S.; Yoshizawa, K.; Iijima, S. *J. Am. Chem. Soc.* **2005**, *127*, 11769−11776.

(50) Koch, W.; Holthausen, M. C. *A Chemist's Guide to Density Functional Theory*; Wiley-VCH: Weinheim, Germany, 2001.

(51) Kolmogorov, A. N.; Crespi, V. H. *Phys. Rev. B* **2005**, *71*, 235415−6.

(52) Yazyev, O. V.; Helm, L. *Phys. Rev. B* **2005**, *72*, 245416.

(53) Cioslowski, J.; Kertesz, M. *J. Chem. Phys.* **1986**, *85*, 7193−7197.